Lattice-Boltzmann modeling of dissolution phenomena

F. Verhaeghe,* S. Arnout,† B. Blanpain, and P. Wollants
Department of Metallurgy and Materials Engineering, Katholieke Universiteit Leuven, Belgium
(Received 20 October 2005; published 28 March 2006)

In this work, we present a lattice-Boltzmann model for the simulation of complex dissolution phenomena. We design boundary conditions to impose a fixed concentration or a surface flux for use in multicomponent lattice-Boltzmann models. These conditions can be applied to simulate complex reactive flow phenomena, e.g., in porous media. By combining the boundary conditions with a volume-of-fluid description of solid structures, the application area of the presented model is extended toward complex dissolution phenomena. The boundary conditions and the dissolution model are validated using benchmark problems with analytical solutions. The agreement is good in all tested cases.

DOI: 10.1103/PhysRevE.73.036316 PACS number(s): 47.10.−g, 47.11.−j, 05.20.Dd

I. INTRODUCTION

Dissolution phenomena are frequently encountered in science and engineering: dissolution of rock formations, drug delivery devices, functional degradation of biodegradable implants, the in-use dissolution of refractory bricks caused by the infiltration of aggressive oxidic liquids, and dissolution of second-phase precipitates in metals, to name but a few. In the past this variety of phenomena has been modeled using an even broader range of approaches, ranging from analytical models [1–3] to numerical simulation both at the macroscopic or Darcy scale [2,4–8] and at the pore scale [9–11].

Over the last two decades, the lattice-Boltzmann method (LBM) [12–20] has evolved into a viable numerical tool for the simulation of complex flow-related phenomena such as multiphase [21–24] and multicomponent flows [25–27], flows through porous media [19], and particulate suspensions in fluid flows [28]. The LBM has also been successfully applied to the simulation of chemically reactive fluids. A great deal of effort has been put into work on bulk chemical reactions [29–33]. In this work, however, we focus on surface reactions and the subsequent dissolution processes.

Wells and co-workers [34] presented a lattice gas automata (LGA) model coupling solute transport with chemical reactions at mineral surfaces and in pore networks. By assigning the mean concentration of a node to each particle at that node and by calculating the new mean concentration from the arriving particles at the node after streaming, diffusion can be modeled in the LGA framework. Surface reactions are modeled by allowing wall nodes to act as sinks or sources of mass with a certain probability depending on the concentration. These wall nodes may become fluid nodes after a large number of events, the number depending on the relative concentrations in solvent and solid phase. Other LGA studies of dissolution phenomena can be found in [35–38].

Kelemen and co-workers [39] extended the lattice Bhatnagar-Gross-Krook (BGK) Eq.(13) with a dissolution boundary condition: when colliding with the wall, the fluid particle has the probability of detaching a solid particle:

$$P = \left(1 - \frac{C}{C_{eq}}\right)\left(\frac{(n-s)}{n}\right) \tag{1}$$

in which C is the solute concentration in the fluid, C_{eq} is the equilibrium concentration of the solute in the fluid, and the final term is a surface tension or chemical potential gradient effect, with n the total number of nearest neighbors and s the number of solid nearest neighbors. The authors used this model to investigate the effect of the Péclet number on the evolution of the structure of a porous medium with partial solubility in the liquid.

He and co-workers [40] tackled diffusion-convection systems with a surface reaction using two sets of populations: a set to simulate the flow field, and a set for the description of the diffusion-convection behavior of the solute. The solute is assumed not to influence the flow field. At the solid surface a general boundary condition capable of imposing a flux or a concentration is imposed, based on the heuristic observation that at a stationary wall the nonequilibrium part of the distribution function is proportional to the scalar product of its microscopic velocity and the concentration gradient. The model is validated using the Lévêque solution [41] and the agreement is good. Kang and co-workers [42,43] used the approach of He *et al.* [40] to simulate chemical dissolution in porous media. Unfortunately no clear description is given on how the solid surface is described and how its movement is calculated from the surface reaction.

Verberg and Ladd [44] designed an algorithm for simulation of chemical erosion in rough fractures consisting of three separate calculations. An optimized lattice-Boltzmann scheme [45] is used to solve the time-independent Stokes flow equations. A continuous bounce-back scheme [45] allows for the boundary to be located anywhere between two grid nodes. In a second calculation the steady-state concentration and flux field are determined through a stochastic solution of the diffusion-convection equation. In the last step the new solid structure is determined based on the local flux of tracer particles across the solid surface, where the assumption is made that the reaction kinetics are instantaneous and

*Electronic mail: Frederik.Verhaeghe@mtm.kuleuven.be
†Electronic mail: Sander.Arnout@mtm.kuleuven.be

that the dissolution is therefore diffusion controlled. Because of the gain in efficiency due to the continuous boundary condition and the implicit method to calculate the Stokes flow, the authors were able to simulate realistic acid erosion phenomena in Carrara marble in qualitative agreement with experimental observations.

O'Brien and co-workers [46] adopted a similar approach as Verberg and Ladd [44] insofar as they also use a lattice-Boltzmann scheme for the calculation of the flow field in porous media using a porous medium no-slip boundary condition [47]. This is combined with a solution of the convection-diffusion equation for the solute transport and reaction-controlled reaction mechanism at the solid interfaces based on species activities rather than concentrations. The model was validated using experimental flow-through experiments with satisfactory agreement. The authors applied their model to a long-term alteration of a rock over a period of several 10 000 years. The results were classified as reasonable.

In this work we design boundary conditions to impose a concentration or a flux on a solid interface for use in multicomponent lattice-Boltzmann models. We will present boundary conditions for multicomponent models using one population per species (see, e.g., [21,22,25,26,48,49]. Free-energy-based models [27] are not considered here. The boundary conditions we present can be used as such, for example to simulate reactive multicomponent flow in porous media. However, we will use them within a model to describe complex dissolution phenomena involving arbitrarily shaped solids in multicomponent liquids. This paper is a detailed follow-up and extension of our previous work: we provide a more profound basis of the concentration boundary condition presented in [50] and we extend the model with an imposed flux boundary condition in order to model reaction-controlled dissolution. The paper is organized as follows. Section II discusses the basic dissolution mechanisms. These are translated into a lattice-Boltzmann model in Sec. III, including the discussion of the concentration and the flux boundary condition. The model is validated using problems with analytical solutions in Sec. IV. In Sec. V some preliminary results are presented. Section VI concludes the paper.

II. DISSOLUTION MECHANISMS

Consider a system with two components A and B obeying the thermodynamics of the phase diagram given in Fig. 1. Assume a solid structure consisting of phase β and saturated with A[1] so that $x_A^{\beta}=x_A^{S,eq}=1-x_B^{S,eq}$, is put into contact with a liquid phase of a certain composition. If the concentration of the liquid is lower than the saturation concentration $x_B^{L,eq}$, the solid will have a tendency to dissolve. The rate of this dissolution process will depend on the reaction kinetics of the dissolution reaction at the solid-liquid interface, and on the diffusion in the liquid. If the reaction kinetics are substantially faster, the diffusion flux limits the dissolution rate because this flux is insufficient to move the excess of B, injected as the solid dissolves, away from the interface. If the diffusion is so fast that there is no pile-up at the interface, the reaction kinetics will control the dissolution rate. In what follows these two limiting situations will be discussed in more mathematical detail.

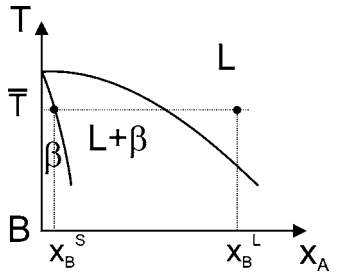

FIG. 1. Simplified phase diagram for the dissolution of a solid phase β with solubility $x_A^{S,eq}=1-x_B^{S,eq}$ for A in a liquid with a solubility limit $x_B^{L,eq}$ for B at a certain temperature $\bar{T}$.

A. General case

In general there will not be one rate-determining process. The dissolution rate will depend on both reaction kinetics and diffusion rate. We can describe the dissolution rate by the flux of B through the interface, which is proportional to the dissolution rate. As a result of the reaction, there will be an incoming flux at the interface, which for first-order reaction kinetics is proportional to the driving force for dissolution, i.e., the difference between the equilibrium concentration x_B^{eq} and the actual concentration at the interface x_B^i (the superscript L is dropped for reasons of clarity):

$$J_R = k(x_B^{eq} - x_B^i)\rho \tag{2}$$

which is a flux per unit area in the direction normal to the surface. This incoming mass is transported away from the interface according to the diffusion flux

$$J_D = D\,(\nabla x_B)|_i \approx \frac{D}{\delta}(x_B^i - x_B^{bulk})\rho \tag{3}$$

in which the concentration gradient has been linearly approximated between the concentration at the interface and the bulk concentration over a diffusion boundary of thickness δ. At the interface the following relation holds [51]:

$$J_R = J_D. \tag{4}$$

From this equality the interface concentration can be calculated:

$$x_B^i = \frac{kx_B^{eq} + D/\delta x_B^{bulk}}{k + D/\delta}. \tag{5}$$

From this the flux at the interface can be calculated:

$$J_R = J_D = \frac{(D/\delta)k}{(D/\delta)+k}(x_B^{eq} - x_B^{bulk})\rho. \tag{6}$$

In the following two subsections, two limiting situations are discussed.

[1]We choose a saturated solid phase for the sake of clear explanation. If the solid is undersaturated, diffusion has also to be considered in the solid phase. This extension can be made in a straightforward way.

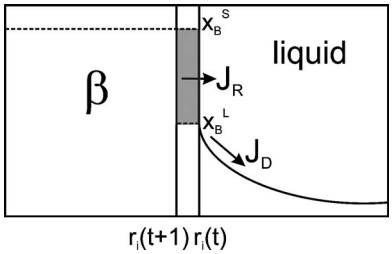

FIG. 2. Schematic representation of diffusion-controlled dissolution: the excess of B (gray-shaded area), proportional to the difference in concentration of B $(x_B^S - x_B^L)$ in solid and liquid, respectively, is transported away from the interface via the diffusion flux J_D.

B. Diffusion-controlled dissolution

If the reaction kinetics can be assumed to be instantaneous compared to the diffusion rate, i.e., $D/\delta \ll k$, the concentration at the interface will be equal to the equilibrium concentration $x_B^{L,eq}$, as can be seen from Eq. (5). In order for the interface to move, the excess of B injected as the solid dissolves has to be transported toward the bulk, which leads to the following rate equation:

$$(x_B^{S,eq} - x_B^{L,eq})\rho \frac{dr_i}{dt} = J_D = (D \nabla x_B^L \rho)_{r=r_i}. \tag{7}$$

This dissolution principle is shown schematically in Fig. 2.

C. Reaction-controlled dissolution

If the diffusion kinetics are substantially faster than the reaction kinetics, i.e., $k \ll D/\delta$, any pile-up at the interface will be flattened out, so that the interface concentration will be equal to the bulk concentration, as can be seen from Eq. (5). In this case the dissolution rate is governed by the reaction kinetics. The reaction-controlled flux can be related to the dissolution rate as follows:

$$(x_B^{S,eq} - x_B^{L,bulk})\rho \frac{dr_i}{dt} = J_R = k(x_B^{L,eq} - x_B^{L,bulk})\rho. \tag{8}$$

In the case of a large surrounding amount of liquid, the bulk concentration $x_B^{L,bulk}$ will remain quasiconstant, so that the dissolution rate per unit area will be constant.

III. LATTICE-BOLTZMANN DISSOLUTION MODEL

A. Lattice-Boltzmann models for binary mixtures

In the past several approaches have been proposed to model multicomponent liquids within a lattice-Boltzmann framework (see, e.g., [21,25,27,48,52] and references therein). In this work we apply the developed boundary conditions to the model of Shan and Doolen [25] without nonlocal interactions, and to the model of Luo and Girimaji [48,49]. Both models describe these mixtures using one set of distribution functions per species. We give a brief overview of the main characteristics of and differences between the models. For further details we refer to the original publications.

In both models each species evolves according to its own lattice-Boltzmann equation in the typical two-step process of collision

$$\tilde{f}_i^A(\boldsymbol{x},t) = f_i^A(\boldsymbol{x},t) + J_i^A, \tag{9}$$

$$\tilde{f}_i^B(\boldsymbol{x},t) = f_i^B(\boldsymbol{x},t) + J_i^B \tag{10}$$

and streaming

$$f_i^A(\boldsymbol{x} + \boldsymbol{e}_i dt, t + dt) = \tilde{f}_i^A(\boldsymbol{x},t), \tag{11}$$

$$f_i^B(\boldsymbol{x} + \boldsymbol{e}_i dt, t + dt) = \tilde{f}_i^B(\boldsymbol{x},t), \tag{12}$$

in which the $\boldsymbol{e}_i$'s are the lattice velocities and J_i^A and J_i^B the collision terms. The macroscopic quantities are calculated as the moments of the distribution functions

$$\rho_k = \sum_i f_i^k, \tag{13}$$

$$\rho_k \boldsymbol{u}_k = \sum_i f_i^k \boldsymbol{e}_i \tag{14}$$

with $k = A, B$. Mass fractions are defined in the usual way:

$$x_k = \frac{\rho_k}{\rho}. \tag{15}$$

The difference between the two models considered here lies in the collision operators J_i^A and J_i^B. In the model by Shan and Doolen, a BGK collision term is chosen:

$$J_i^A = -\frac{1}{\tau_A}[f_i^A - f_i^{A,eq}(n_A, \boldsymbol{u}')], \tag{16}$$

$$J_i^B = -\frac{1}{\tau_B}[f_i^B - f_i^{B,eq}(n_B, \boldsymbol{u}')], \tag{17}$$

in which both species relax toward an equilibrium distribution function defined in terms of their number densities n^A and n^B and a common velocity $\boldsymbol{u}'$ defined as

$$\boldsymbol{u}' = \sum_\sigma \frac{\rho_\sigma \boldsymbol{u}_\sigma}{\tau_\sigma} \Bigg/ \sum_\sigma \frac{\rho_\sigma}{\tau_\sigma}. \tag{18}$$

Luo and Girimaji [48,49] derived a lattice-Boltzmann model for binary fluids from the kinetic theory model of gas mixtures proposed by Sirovich [53]. In their collision operators, they make a distinction between collisions between like particles, and collisions between unlike particles:

$$J_i^A = J_i^{AA} + J_i^{AB}, \tag{19}$$

$$J_i^B = J_i^{BB} + J_i^{BA}, \tag{20}$$

in which each term is modeled as a BGK collision operator:

$$J_i^{AA} = -\frac{1}{\tau_A}(f_i^A - f_i^{A(0)}), \tag{21}$$

$$J_i^{BB} = -\frac{1}{\tau_B}(f_i^B - f_i^{B(0)}), \tag{22}$$

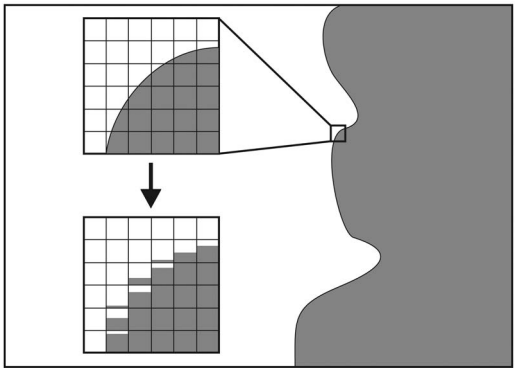

FIG. 3. Example of a geometry for the dissolution simulations. The white areas are liquid, the gray areas solid. The top inset shows how a grid is placed over the geometry. The bottom inset shows the translation into volume fractions of solid.

$$J_i^{AB} = -\frac{1}{\tau_D}\frac{\rho_B}{\rho}\frac{f_i^{Aeq}}{R_A T}(\boldsymbol{e}_i - \boldsymbol{u})\cdot(\boldsymbol{u}_A - \boldsymbol{u}_B), \tag{23}$$

$$J_i^{BA} = -\frac{1}{\tau_D}\frac{\rho_A}{\rho}\frac{f_i^{Beq}}{R_B T}(\boldsymbol{e}_i - \boldsymbol{u})\cdot(\boldsymbol{u}_B - \boldsymbol{u}_A). \tag{24}$$

The properties of the mixture are calculated from those of the species:

$$\rho = \sum_k \rho_k, \tag{25}$$

$$\rho \boldsymbol{u} = \sum_k \rho_k \boldsymbol{u}_k. \tag{26}$$

In the publications about both models the transport coefficients, such as the shear viscosity and the diffusion coeffecients, are derived by means of a Chapman-Enskog expansion and the expressions can be found there. In this work, for the sake of validation, we use diffusion coefficients which are independent of the concentration of the species. For the Shan-Doolen model without nonlocal interactions, this means that the two relaxation times τ_A and τ_B are equal [25]. In this case the model of Shan and Doolen is identical to the model of Luo and Girimaji, if $\tau_A = \tau_B = \tau_D$ is chosen in the latter. The results presented in this paper are obtained with the model of Luo and Girimaji. As a result, however, they are also valid for the model of Shan and Doolen, within the constraints stated above.

B. Geometry

A typical example of a geometry for dissolution simulations is given in Fig. 3. The simulation domain is divided into square calculation cells (top inset of Fig. 3). We employ a volume-of-fluid technique and assign a volume fraction solid a to every cell (bottom inset of Fig. 3). We differentiate between two types of cells: fluid cells ($a < 0.5$) and solid cells ($a \geqslant 0.5$). The lattice-Boltzmann variables are calculated at the center of the cells. For boundary cells (i.e., fluid cells with at least one solid neighbor cell) we define the dimensionless distance q to the interface (per unit lattice distance in the direction under consideration). In general there are two possibilities for fluid cells: the cell can be fully fluid, i.e., $a=0$, or it can be partially solid, i.e., $0 < a < 0.5$. In the former case, the distance q is larger than 0.5. In the latter case, $q < 0.5$. These cases can be seen in Fig. 4 for several directions (diagonal and nondiagonal). The normal vector on the interface can be calculated from the normalized gradient of the volume fraction field (see, e.g., [54]).

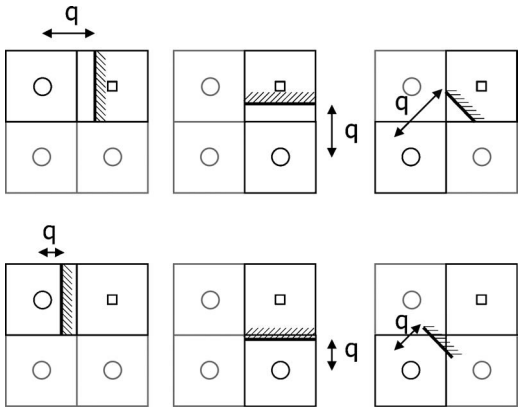

FIG. 4. Examples of the location of the boundary for different populations interacting with the same solid cell. ○ are fluid boundary cells, □ indicate solid cells. (a) Boundary cells with $a=0$ and boundary located at $q \geqslant 0.5$; (b) boundary cells with $0 < a < 0.5$ and boundary located at $q < 0.5$.

C. Boundary conditions

Boundary conditions in lattice-Boltzmann models are fundamentally different from their equivalents for more traditional computational fluid dynamics methods [55]. The populations leaving the domain have to be replaced by populations entering the domain. In general the number of macroscopic conditions on the boundary is insufficient to calculate all incoming populations. Great care has to be taken in the development of boundary conditions for lattice-Boltzmann methods in order to obtain stable simulations.

1. Concentration boundary condition

In order to model diffusion-controlled dissolution we need to be able to impose a fixed concentration at the solid-liquid interface, which in general can be located anywhere between grid points. In this section we describe the special case of a fully fluid node (with $a=0$) with an adjacent fully solid node (with $a=1$), which is shown in Fig. 5(a). Assume that the populations $\tilde{f}_\alpha^A$ and $\tilde{f}_\alpha^B$ are leaving the domain. We want to impose species densities

$$\rho_A = x_A \rho, \tag{27a}$$

$$\rho_B = x_B \rho. \tag{27b}$$

The amount of species A traveling along a pair of opposite directions α and $\bar{\alpha}$ (in what follows called a link) can be expressed as the sum of the known population $\tilde{f}_\alpha^A$ leaving the

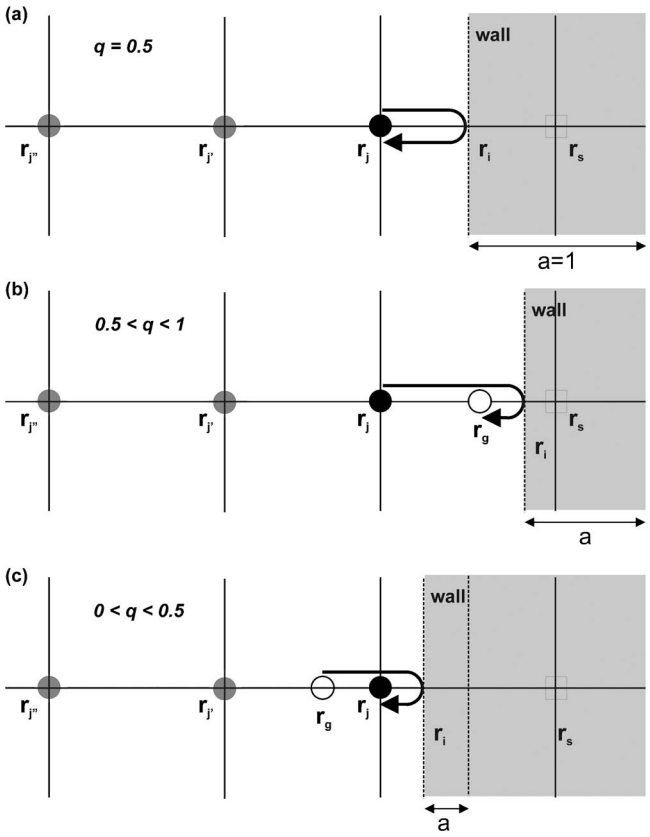

FIG. 5. Schematic of the different cases for the location of the interface. (a) $q=0.5$, (b) $q>0.5$, (c) $0<q<0.5$.

domain and the unknown population $f^A_{\bar{\alpha}}$ entering the domain: $(\tilde{f}^A_\alpha + f^A_{\bar{\alpha}})$. For B this is $(\tilde{f}^B_\alpha + f^B_{\bar{\alpha}})$. The total mass along that link is similarly $(\tilde{f}^A_\alpha + f^A_{\bar{\alpha}} + \tilde{f}^B_\alpha + f^B_{\bar{\alpha}})$. Inserting all these expressions in Eqs. (27) yields

$$\tilde{f}^A_\alpha + f^A_{\bar{\alpha}} = x_A(\tilde{f}^A_\alpha + f^A_{\bar{\alpha}} + \tilde{f}^B_\alpha + f^B_{\bar{\alpha}}), \tag{28a}$$

$$\tilde{f}^B_\alpha + f^B_{\bar{\alpha}} = x_B(\tilde{f}^A_\alpha + f^A_{\bar{\alpha}} + \tilde{f}^B_\alpha + f^B_{\bar{\alpha}}), \tag{28b}$$

which is a system of two dependent equations for two unknown populations $f^B_{\bar{\alpha}}$ and $f^B_{\bar{\alpha}}$. Now we also want to impose a zero-velocity boundary condition at the interface using the classic bounce-back condition (see, e.g., [56]) for the sum of the populations:

$$f^A_{\bar{\alpha}} + f^B_{\bar{\alpha}} = \tilde{f}^A_\alpha + \tilde{f}^B_\alpha. \tag{29}$$

Equation (29) can now be used to decouple the system (28) by inserting it into the right-hand side of the equations:

$$\tilde{f}^A_\alpha + f^A_{\bar{\alpha}} = 2x_A(\tilde{f}^A_\alpha + \tilde{f}^B_\alpha), \tag{30a}$$

$$\tilde{f}^B_\alpha + f^B_{\bar{\alpha}} = 2x_B(\tilde{f}^A_\alpha + \tilde{f}^B_\alpha). \tag{30b}$$

Solving this for the unknown incoming populations $f^A_{\bar{\alpha}}$ and $f^B_{\bar{\alpha}}$ yields the following set of boundary conditions:

$$f^A_{\bar{\alpha}} = 2x_A(\tilde{f}^A_\alpha + \tilde{f}^B_\alpha) - \tilde{f}^A_\alpha, \tag{31a}$$

$$f^B_{\bar{\alpha}} = 2x_B(\tilde{f}^A_\alpha + \tilde{f}^B_\alpha) - \tilde{f}^B_\alpha, \tag{31b}$$

which is the same result as stated in [50]. In general the last fluid node is not located half a lattice spacing from the interface. To apply the boundary conditions in general, an interpolation scheme similar to that reported in [57] is used. This will be discussed in Sec. III C 3.

2. Flux boundary condition

In general, the dissolution rate is dependent on the reaction kinetics and the diffusion rate, and the concentration at the boundary is not known *a priori*. For a first-order reaction, the dissolution rate at the surface is proportional to the driving force, being the difference between the equilibrium concentration and the actual concentration [51]. The flux J_R of B injected when an increment of solid dissolves has to be transported away from the interface by diffusion. It is known from the single-component lattice-Boltzmann models [57] that a flux can be imposed on a surface halfway from the last fluid node through a modification of the bounce-back rule:

$$f^B_{\bar{\alpha}} = \tilde{f}^B_\alpha + 6w_\alpha \mathbf{e}_\alpha \cdot J_R \mathbf{n} \tag{32}$$

with $\mathbf{n}$ the normal vector on the interface. The expression for the flux J_R contains the total and partial densities. These can be calculated from the populations in the following way:

$$w_\alpha \rho = \tfrac{1}{2}(\tilde{f}^A_\alpha + f^A_{\bar{\alpha}} + \tilde{f}^B_\alpha + f^B_{\bar{\alpha}}), \tag{33a}$$

$$w_\alpha \rho_B = \tfrac{1}{2}(\tilde{f}^B_\alpha + f^B_{\bar{\alpha}}). \tag{33b}$$

Substituting expression (2) for the flux J_R, Eqs. (33) and the bounce-back relations (29) yield the following result for the imposed flux boundary condition (32):

$$f^B_{\bar{\alpha}} = \tilde{f}^B_\alpha + 3k[2x_B(\tilde{f}^A_\alpha + \tilde{f}^B_\alpha) - (\tilde{f}^B_\alpha + f^B_{\bar{\alpha}})]\mathbf{e}_\alpha \cdot \mathbf{n} \tag{34}$$

with the rate constant k expressed in lattice units per time step. Solving this equation for the unknown population $f^B_{\bar{\alpha}}$ yields

$$f^B_{\bar{\alpha}} = \frac{k_\alpha}{1+k_\alpha} 2x_B(\tilde{f}^A_\alpha + \tilde{f}^B_\alpha) + \frac{1-k_\alpha}{1+k_\alpha}\tilde{f}^B_\alpha \tag{35}$$

in which $k_\alpha = 3k\mathbf{e}_\alpha \cdot \mathbf{n}$.

Taking the limit of infinitely fast reaction kinetics, i.e., $k \to \infty$, formally confirms the boundary conditions (31) for diffusion control.

3. Interpolation scheme

Since the diffusion-controlled case is a special case of the mixed control case (namely, the limit for infinitely fast reaction kinetics), we describe the interpolation procedure for the latter and perform the derivation for species B; the same can easily be repeated for species A.

Two different cases, which are depicted in Fig. 5, are considered: (b) the boundary is located between half a lattice

spacing and one lattice spacing and (c) the boundary is located at less than half a lattice spacing from the boundary node. In case (b) a ghost node r_g is created so that populations moving toward the interface and originating from the fluid node r_j closest to the interface end up as populations in this ghost node:

$$f^B_{\bar{\alpha}}(r_g) = \frac{k_\alpha}{1+k_\alpha} 2x_B[\tilde{f}^A_\alpha(r_j) + \tilde{f}^B_\alpha(r_j)] + \frac{1-k_\alpha}{1+k_\alpha}\tilde{f}^B_\alpha(r_j). \quad (36)$$

This is also indicated by the arrow in Fig. 5(b). After the application of the boundary condition the unknown population moving away from the interface in the fluid node r_j closest to the interface can be interpolated from the known populations at the neighboring nodes r_j' and r_j'' and the ghost node r_g:

$$f^B_{\bar{\alpha}}(r_j) = \frac{1}{q(2q+1)} f^B_{\bar{\alpha}}(r_g) + \frac{2q-1}{q} f^B_{\bar{\alpha}}(r_{j'}) - \frac{2q-1}{2q+1} f^B_{\bar{\alpha}}(r_{j''}). \quad (37)$$

In case (c) the boundary is located at $q<0.5$. In this case a ghost node r_g is created so that populations at this ghost node move toward the interface and end up as populations in the boundary node r_j. The populations in the ghost node can be calculated through interpolation from the values in the neighboring nodes r_j, r_j' and r_j'':

$$\tilde{f}^B_\alpha(r_g) = q(1+2q)\tilde{f}^B_\alpha(r_j) - q(1-4q^2)\tilde{f}^B_\alpha(r_{j'}) - q(1-2q)\tilde{f}^B_\alpha(r_{j''}). \quad (38)$$

With this expression and the boundary condition (36) the populations can be calculated at the boundary node:

$$f^B_{\bar{\alpha}}(r_j) = \frac{k_\alpha}{1+k_\alpha} 2x_B[\tilde{f}^A_\alpha(r_g) + \tilde{f}^B_\alpha(r_g)] + \frac{1-k_\alpha}{1+k_\alpha}\tilde{f}^B_\alpha(r_g). \quad (39)$$

D. Evolution of solid structure

With the boundary conditions described above it is possible to calculate the incoming populations from the populations leaving the domain and the macroscopic properties that have to be imposed. To simulate dissolution phenomena, a scheme has to be designed to update the solid structure accordingly. The amount of species B injected in the system can be calculated from the difference between populations leaving and entering the system. The amount of dissolved solid is then equal to the amount of injected B divided by the difference between the solid concentration $x_B^{eq,S}$ and the actual concentration B in the cell:

$$\frac{da}{dt} = \sum_{nb} \frac{\tilde{f}^B_\alpha - f^B_{\bar{\alpha}}}{x_B^{eq,S} - x_B^L}, \quad (40)$$

where the summation is made over all fluid cells neighboring (nb) the fluid (if $a>0$) or solid cell under consideration. In the case of diffusion-controlled dissolution, the concentration on the interface is known, so in this case $x_B^L = x_B^{eq,L}$. In the case of reaction-controlled dissolution, however, the actual concentration on the interface is not known. In order to avoid extrapolation to the interface of the concentration at the nearest fluid nodes, we use the following expression:

$$x_B^L = \frac{\tilde{f}^B_\alpha + f^B_{\bar{\alpha}}}{\tilde{f}^A_\alpha + f^A_{\bar{\alpha}} + \tilde{f}^B_\alpha + f^B_{\bar{\alpha}}}. \quad (41)$$

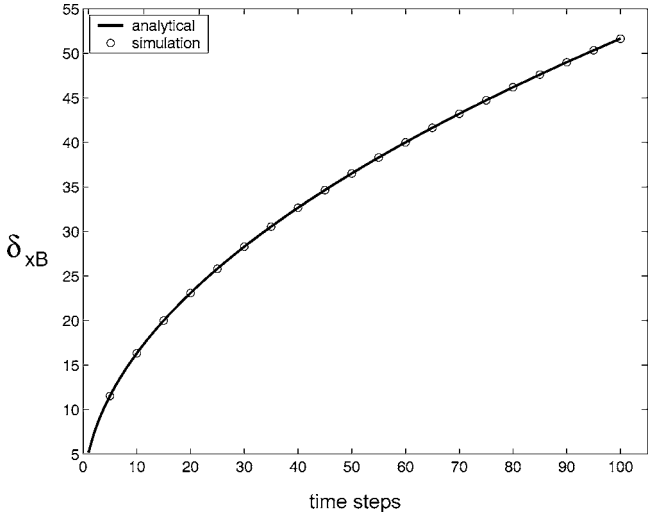

FIG. 6. Comparison of the analytical penetration depth δ_{x_B} with the simulated result for a one-dimensional transient mass transfer problem.

IV. VALIDATION

A. Concentration boundary condition

To quantitatively validate the presented concentration boundary condition we simulated penetration into a semi-infinite medium. The governing macroscopic equation is

$$\partial_t x_B(r,t) = D\nabla^2 x_B(x,t) \quad (42)$$

with initial and boundary conditions

$$x_B(x,0) = x_{B,0}, \quad (43a)$$

$$x_B(0,t) = x_{B,1}, \quad (43b)$$

$$x_B(\infty,t) = x_{B,0}. \quad (43c)$$

This problem can be solved analytically [58] and the concentration profile is given by

$$\frac{x_B - x_{B,0}}{x_{B,1} - x_{B,0}} = 1 - \mathrm{erf}\left(\frac{r}{2\sqrt{(Dt)}}\right). \quad (44)$$

For this problem a penetration depth δ_{x_B} is typically defined as

$$\delta_{x_B} = 4\sqrt{Dt} \quad (45)$$

which is the distance at which less than 1% of the concentration difference $x_{B,1} - x_{B,0}$ has been reached at a certain time. In Fig. 6 the comparison of this analytical expression

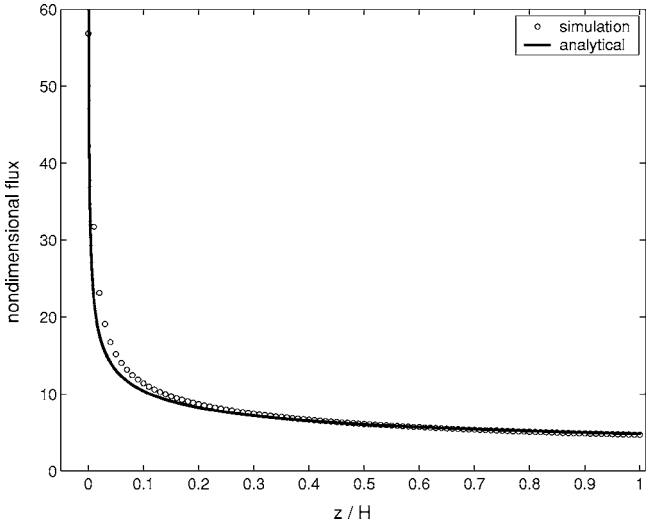

FIG. 7. Comparison of the simulated flux and the analytical expression as a function of the normalized streamwise coordinate for a Péclet number of Pe=178 for the Lévêque problem.

for δ_{x_B} with the simulated result is made and the agreement is satisfactory.

A challenging test case for the concentration boundary condition under convective conditions is the Lévêque problem [41]. The problem setup is the following. A solution is forced by a pressure difference to flow between two parallel plates. The top surface does not react with the solution, imposing a no-flux condition. At the bottom surface a concentration $x_B=0$ of B, different from the inflow concentration x_B^0 of the liquid, is imposed. For large Péclet numbers, defined as $\mathrm{Pe}=U_c H/D$ with U_c the centerline velocity, H the height of the channel, and D the diffusion coefficient, the flux of B through the surface can be expressed as

$$\frac{H}{x_B^0}\frac{\partial x_B}{\partial n} = \frac{1}{\Gamma(4/3)9^{1/3}}\left(\frac{4\mathrm{Pe}}{z/H}\right) \tag{46}$$

with Γ the Gamma function and z the streamwise coordinate. Figure 7 shows the comparison of the simulated flux and the analytical expression as a function of the normalized streamwise coordinate. The agreement is good, especially considering the fact that the analytical expression for the flux exhibits a singularity at $z=0$.

B. Diffusion-controlled dissolution of a planar front

The diffusion-controlled dissolution of a solid with a planar front is a moving boundary problem with an analytical solution. The boundary condition (43b) has to be replaced by the Stefan conditions

$$(D\nabla x_B)_{r=r_i} = (1-x_{B,1})\frac{dr_i}{dt}, \tag{47}$$

$$x_B(r_i,t) = x_{B,1}, \tag{48}$$

with $r_i(t)$ the location of the interface at a given time t. The solution for X is given by [59]

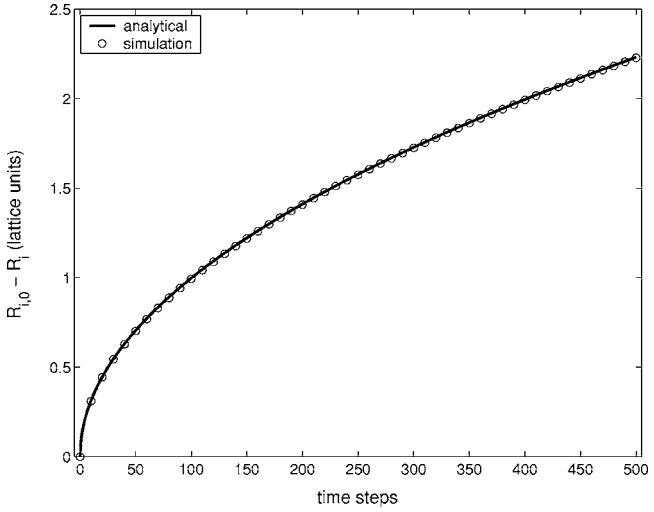

FIG. 8. Comparison of analytical position and the simulated result of a planar interface dissolving under diffusion control.

$$r_{i,0} - r_i = L\sqrt{Dt} \tag{49}$$

with $r_{i,0}$ the initial position of the interface, and L a constant. The comparison with the simulation result is given in Fig. 8 and is excellent.

C. Reaction-controlled dissolution of a planar front

The reaction-controlled dissolution of a solid with a planar front allows us to quantitatively validate the reaction-controlled dissolution model. In order to simulate reaction-control, k has to be small compared to the diffusion coefficient D. The movement of the interface can be described using Eq. (8). Integrating this equation yields the following expression for the position r_i of the interface as a function of time:

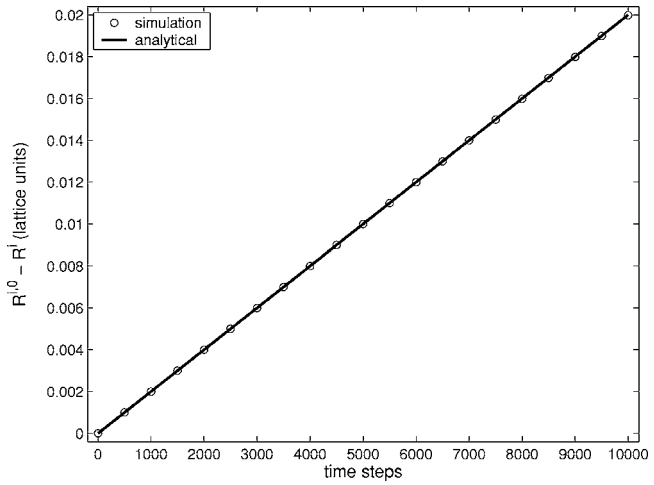

FIG. 9. Comparison of analytical position of the interface with the simulated result for reaction control with a rate constant $k=10^{-5}$.

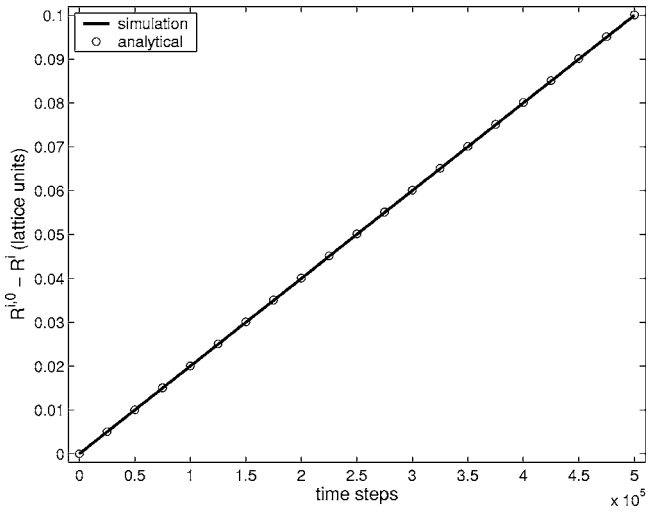

FIG. 10. Comparison of analytical position of a cylindrical interface with the simulated result for a rate constant $k=10^{-6}$, $x_B^{L,eq}-x_B^{L,i}=0.5$, $x_B^{S,eq}-x_B^{L,i}=0.1$, and 5×10^5 time steps.

$$r_{i,0}-r_i=\left(\frac{x_B^{L,eq}-x_B^{L,i}}{x_B^{S,\mathrm{eq}}-x_B^{L,i}}\right)kt \tag{50}$$

with $r_{i,0}$ the initial position of the interface. Figure 9 shows the comparison between the analytical position of the interface and the simulation results for a rate constant $k=10^{-5}$. The agreement is excellent.

D. Reaction-controlled dissolution of a cylinder

Assuming that the diffusion is fast enough to keep the concentration x_B^i of the liquid approximately constant at the interface, the dissolution rate of a cylinder with initial radius $r_{i,0}$ can be expressed as [51]

$$-(x_B^{S,eq}-x_B^{L,i})\frac{dV}{dt}=kA(x_B^{L,eq}-x_B^{L,i}) \tag{51}$$

with $V=\pi r_i^2$ and $A=2\pi r_i$ the volume and the surface of the cylinder per unit length, respectively, and $r_i(t)$ the time-dependent radius of the cylinder. Inserting these expressions in the rate Eq. (51) yields after simplification

$$-(x_B^{S,eq}-x_B^{L,i})\frac{dr}{dt}=k(x_B^{L,eq}-x_B^{L,i}) \tag{52}$$

which can be rewritten as

$$-dr=\left(\frac{x_B^{S,eq}-x_B^{L,i}}{x_B^{L,eq}-x_B^{L,i}}\right)k\,dt. \tag{53}$$

Integrating this yields

$$r_0-r=\left(\frac{x_B^{S,eq}-x_B^{L,i}}{x_B^{L,eq}-x_B^{L,i}}\right)kt \tag{54}$$

so the radius of the cylinder varies linearly with time. Figure 10 shows the comparison between simulation and theory for a cylinder of initial radius 20 lattice units on a grid of 100×100 cells, with $x_B^{L,eq}-x_B^{L,i}=0.5$, $x_B^{S,eq}-x_B^{L,i}=0.1$, $k=10^{-6}$, and 5×10^5 time steps. The agreement is again very good.

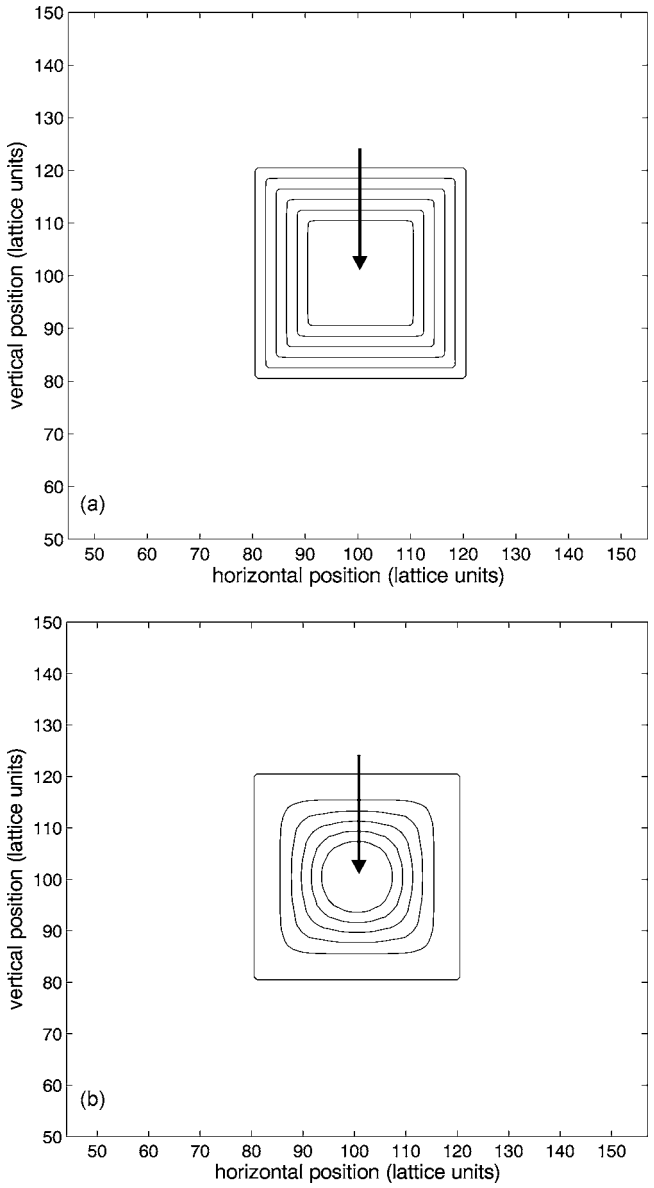

FIG. 11. Dissolution behavior of a square cylinder. The arrow indicates the direction of movement of the front. (a) In the case of reaction-control, the front remains square due to the constant driving force per unit surface. (b) In the case of diffusion control, the system tries to minimize the surface per volume and the front rounds.

V. RESULTS

To show the potentiality of the proposed model, we simulate the dissolution behavior of a square cylinder. The square has a size of 40×40 lattice units in a domain of 200×200 lattice units. Two simulations are performed: one in which the dissolution is diffusion controlled, the other in which the dissolution is reaction controlled. The resulting geometrical evolution of the solid interface with time is depicted in Fig. 11. In the case of reaction control [Fig. 11(a)], the driving

force per unit surface is constant and the front remains square. When the dissolution is diffusion controlled, however [Fig. 11(b)], the system evolves toward a minimal surface per unit volume and the interface rounds.

VI. CONCLUSIONS

In this paper, we presented boundary conditions to impose a concentration or a flux on a solid interface in multicomponent lattice-Boltzmann models using a set of populations for every species. We have taken the model Shan and Doolen, and the model of Luo and Girimaji as examples. The proposed boundary conditions can be used without the dissolution model, e.g., to describe porous media with a surface reaction that does not affect the structure. However, we included these boundary conditions into a broader model to describe the complex phenomena occurring when an arbitrarily shaped solid is brought into contact with a multicomponent liquid.

The main difference from previous lattice-Boltzmann models is the fact that the dissolution phenomena are described within the framework of a multicomponent model, whereas other authors [42,43] have mainly used a separate set of populations for the fluid flow and for the convection-diffusion of the solute, making the assumption that the solute does not influence the flow. For the same number of variables, namely, two sets of populations, we do not make this assumption. It should be noted, however, that due to the BGK assumption in the collision terms, the stability of the model limits the achievable Schmidt and Péclet numbers. A formulation with multiple relaxation times might relax this constraint. It should also be remarked that for the sake of validation we have only considered constant diffusion coefficients, limiting the simulations to linear diffusion problems. A next step will be to test the boundary conditions in available models accounting for nonideal behavior.

With our model it is possible to simulate both diffusion- and reaction-controlled dissolution as limiting situations, and mixed-control dissolution in general. The boundary conditions and the dissolution model as a whole have been thoroughly validated using problems with an analytical solution. In all cases the agreement is good. As an example of the potentiality of the method, the geometrical evolution of the interface of an initially square cylinder is simulated for both reaction control and diffusion control. The results are as would be expected.

ACKNOWLEDGMENTS

F.V. would like to acknowledge the support of the Research Foundation Flanders (FWO Vlaanderen). This research is partially funded by the IWT (Institute for Science and Technology) Project No. 030880.

[1] J. Chadam, D. Hoff, E. Merino, P. Ortoleva, and P. Sen, J. Appl. Math. **36**, 207 (1986).
[2] E. Aharonov, J. Whitehead, P. Kelemen, and M. Spiegelman, J. Geophys. Res. **100**, 20433 (1995).
[3] P. Dijk and B. Berkowitz, Water Resour. Res. **34**, 457 (1998).
[4] P. Lichtner, in *Reactive Transport in Porous Media* (Mineralogical Society of America, Washington, 1996), Vol. 34, pp. 1–81.
[5] C. Wei and P. Ortoleva, Earth-Sci. Rev. **29**, 183 (1990).
[6] E. Aharonov, M. Spiegelman, and P. Kelemen, J. Geophys. Res. **102**, 14821 (1997).
[7] X. Liu, A. Ormond, K. Bartko, Y. Li, and P. Ortoleva, J. Pet. Sci. Eng. **17**, 181 (1997).
[8] A. Ormond and P. Ortoleva, J. Geophys. Res. **105**, 16737 (2000).
[9] S. Békri, J. Thovert, and P. Adler, Chem. Eng. Sci. **50**, 2765 (1995).
[10] J. Sallès, J. Thovert, and P. Adler, Chem. Eng. Sci. **48**, 2839 (1993).
[11] S. Békri, J. Thovert, and P. Adler, Eng. Geol. (Amsterdam) **48**, 283 (1997).
[12] G. R. McNamara and G. Zanetti, Phys. Rev. Lett. **61**, 2332 (1988).
[13] Y. Qian, D. D'Humieres, and P. Lallemand, Europhys. Lett. **17**, 479 (1992).
[14] H. Chen, S. Chen, and W. Matthaeus, Phys. Rev. A **45**, R5339 (1992).
[15] D. D'Humieres, in *AIAA Rarefied Gas Dynamics: Theory and Simuations*, edited by B. D. Shizgal and D. P. Weaver, Progress in Astronautics and Aeronautics, Vol. 59 (AIAA, Washington, D.C., 1992).
[16] X. He and L.-S. Luo, Phys. Rev. E **55**, R6333 (1997).
[17] X. He and L.-S. Luo, Phys. Rev. E **56**, 6811 (1997).
[18] X. Shan and X. He, Phys. Rev. Lett. **80**, 65 (1998).
[19] S. Chen and G. Doolen, Annu. Rev. Fluid Mech. **30**, 329 (1998).
[20] D. Wolf-Gladrow, *Lattice-Gas Cellular Automata and Lattice Boltzmann Models*, Lecture Notes in Mathematics, Vol. 1725 (Springer-Verlag, Berlin, 2000).
[21] X. Shan and H. Chen, Phys. Rev. E **47**, 1815 (1993).
[22] X. Shan and H. Chen, Phys. Rev. E **49**, 2941 (1994).
[23] L.-S. Luo, Phys. Rev. Lett. **81**, 1618 (1998).
[24] L.-S. Luo, Phys. Rev. E **62**, 4982 (2000).
[25] X. Shan and G. D. Doolen, J. Stat. Phys. **81**, 379 (1995).
[26] X. Shan and G. Doolen, Phys. Rev. E **54**, 3614 (1996).
[27] M. R. Swift, E. Orlandini, W. R. Osborn, and J. M. Yeomans, Phys. Rev. E **54**, 5041 (1996).
[28] D. Qi, J. Fluid Mech. **385**, 43 (1999).
[29] R. Kingdon and P. Schofield, J. Phys. A **25**, L907 (1992).
[30] S. P. Dawson, S. Chen, and G. Doolen, J. Chem. Phys. **98**, 1514 (1993).
[31] Y. Qian and S. Orszag, J. Stat. Phys. **81**, 237 (1995).
[32] S. Chen, S. Dawson, G. Doolen, D. Janecky, and A. Lawniczak, Comput. Chem. Eng. **19**, 617 (1995).
[33] J. Weimar and J.-P. Boon, Physica A **224**, 207 (1996).
[34] J. Wells, D. Janecky, and B. Travis, Physica D **47**, 115 (1991).

[35] L. B. Kier and C.-K. Cheng, Pharm. Res. **12**, 1521 (1995).
[36] A. S. McLeod, S. Bordia, and L. F. Gladden, Europhys. Lett. **46**, 571 (1999).
[37] B. Chopard, A. Masselot, and A. Dupuis, Comput. Phys. Commun. **129**, 167 (2000).
[38] M. Johns and L. Gladden, Phys. Fluids **14**, 4152 (2002).
[39] P. Kelemen, J. Whitehead, E. Ahanorov, and K. Jordahl, J. Geophys. Res. **100**, 475 (1995).
[40] X. He, N. Li, and B. Goldstein, Mol. Simul. **25**, 145 (2000).
[41] M. A. Lévêque, Ann. Mines **13**, 284 (1928).
[42] Q. Kang, D. Zhang, and S. Chen, Phys. Rev. E **65**, 036318 (2002).
[43] Q. Kang, D. Zhang, and S. Chen, J. Geophys. Res. **108**, 9 (2003).
[44] R. Verberg and A. J. C. Ladd, Phys. Rev. E **65**, 056311 (2002).
[45] R. Verberg and A. J. C. Ladd, Phys. Rev. Lett. **84**, 2148 (2000).
[46] G. O'Brien, C. Bean, and F. McDermott, J. Hydrol. **268**, 143 (2002).
[47] O. Dardis and J. McCloskey, Phys. Rev. E **57**, 4834 (1998).
[48] L.-S. Luo and S. S. Girimaji, Phys. Rev. E **66**, 035301(R) (2002).
[49] L.-S. Luo and S. S. Girimaji, Phys. Rev. E **67**, 036302 (2003).
[50] F. Verhaeghe, S. Arnout, B. Blanpain, and P. Wollants, Phys. Rev. E **72**, 036308(R) (2005).
[51] F. Habashi, *Principles of Extractive Metallurgy* (Gordon and Breach, New York, 1969).
[52] P. Asinari, Phys. Fluids **17**, 067102 (2005).
[53] L. Sirovich, Phys. Fluids **5**, 908 (1962).
[54] R. Scardovello and S. Zaleski, Annu. Rev. Fluid Mech. **31**, 567 (1999).
[55] I. Ginzburg and D. d'Humières, Phys. Rev. E **68**, 066614 (2003).
[56] X. He, Q. Zou, L.-S. Luo, and M. Dembo, J. Stat. Phys. **87**, 115 (1997).
[57] M. Bouzidi, M. Firdaouss, and P. Lallemand, Phys. Fluids **13**, 3452 (2001).
[58] R. B. Bird, W. E. Stewart, and E. N. Lightfoot, *Transport Phenomena*, 2nd ed. (Wiley, New York, 2002).
[59] H. B. Aaron, D. Fainstein, and G. R. Kotler, J. Appl. Phys. **41**, 4404 (1970).